Available online at www.sciencedirect.com
ScienceDirect
Journal of Molecular Graphics and Modelling 25 (2007) 784–793
Journal of Molecular Graphics and Modelling
www.elsevier.com/locate/JMGM

Contributions of 3′-overhang to the dissociation of small interfering RNAs from the PAZ domain: Molecular dynamics simulation study

Hui Sun Lee [a,d], Soo Nam Lee [b,d], Chul Hyun Joo [a,d], Heuiran Lee [a,d], Han Saem Lee [b,d], Seung Yong Yoon [c,d], Yoo Kyum Kim [a,d,*], Han Choe [b,d,*]

[a] Department of Microbiology, University of Ulsan College of Medicine, 388-1 PoongNap-dong Songpa-goo, Seoul 138-736, South Korea
[b] Department of Physiology, University of Ulsan College of Medicine, 388-1 PoongNap-dong Songpa-goo, Seoul 138-736, South Korea
[c] Department of Anatomy and Cell Biology, University of Ulsan College of Medicine, 388-1 PoongNap-dong Songpa-goo, Seoul 138-736, South Korea
[d] Research Institute for Biomacromolecules, University of Ulsan College of Medicine, 388-1 PoongNap-dong Songpa-goo, Seoul 138-736, South Korea

Received 18 March 2006; received in revised form 3 July 2006; accepted 4 July 2006
Available online 11 July 2006

Abstract

RNA interference (RNAi) is a ‘knock-down’ reaction to reduce expression of a specific gene through highly regulated, enzyme-mediated processes. Small interfering RNAs (siRNAs) are RNA molecules that play an effector role in RNAi and can bind the PAZ domains present in Dicer and RISC. We investigated the interaction between the PAZ domain and the siRNA-like duplexes through dissociation molecular dynamics (DMD) simulations. Specifically, we focused on the response of the PAZ domain to various 3′-overhang structures of the siRNA-like duplexes. We found that the siRNA-like duplex with the 3′ UU-overhang made relatively more stable complex with the PAZ domain compared to those with 3′ CC-, AA-, and GG-overhangs. The siRNA-like duplex with UU-overhang was easily dissociated from the PAZ domain once the structural stability of the complex is impaired. Interestingly, the 3′ UU-overhang spent the least time at the periphery region of the binding pocket during the dissociation process, which can be mainly attributable to UU-overhang’s smallest number of hydrogen bonds.

Keywords: RNA interference; Small interfering RNA; PAZ domain; Molecular recognition; Molecular dynamics simulation

1. Introduction

In diverse eukaryotes, double-stranded RNA (dsRNA) triggers the destruction of mRNA sharing sequence with the double strand. In animals and basal eukaryotes, this process is called RNA interference (RNAi) [1]. RNAi is initiated by short dsRNA products of 21–25 nt, called small interfering RNAs (siRNAs), fragmented from a long dsRNA by the multidomain RNase III enzyme, Dicer [2,3]. The introduction of chemically synthesized, ∼21 nt siRNAs into cells also can facilitate the degradation of homologous RNAs. Synthetic or natural siRNA is a dsRNA in which the double helix is bounded by 2 nt 3′-overhangs [4–6]. Subsequently, siRNAs serve as the substrate selectors for the RNAi within a protein complex called RNA-induced silencing complex (RISC) [7].

RISC consists of protein components and a single-stranded version of siRNA [8]. A siRNA in RISC recognizes specific sequences of mRNA through base pairing, before the homologous target mRNA is cleaved. The signature element of a RISC is an Argonaute protein that has PAZ and PIWI domains [9]. The crystal structure of Argonaute demonstrated that the PIWI domain is similar to ribonuclease H, strongly implicating that an Argonaute protein is the ‘‘Slicer’’ of the target RNAs [10].

It is known that siRNA can bind to the PAZ domain (the proteins Piwi, Argonaute and Zwille) which is also found in a Dicer [11]. A crystal structure of a PAZ domain shows that the PAZ domain has a left-handed, β-barrel core structure (Fig. 1a) [12,13]. The PAZ domain consists of two sub-domains. One sub-domain is similar to the OB fold, albeit with a different topology, which is a single-stranded nucleic acid binding fold. The second sub-domain is composed of a β-hairpin followed by an α-helix. The PAZ domain interacts with the 3′-overhang of RNA in the RNA-binding pocket, which is a cleft between the two sub-domains. The RNA-binding pocket is generated by

* Corresponding authors. Tel.: +82 2 3010 4292; fax: +82 2 3010 8119.
E-mail addresses: ykkim@amc.seoul.kr (Y.K. Kim), hchoe@amc.seoul.kr (H. Choe).

1093-3263/$ – see front matter © 2006 Elsevier Inc. All rights reserved.
doi:10.1016/j.jmgm.2006.07.002

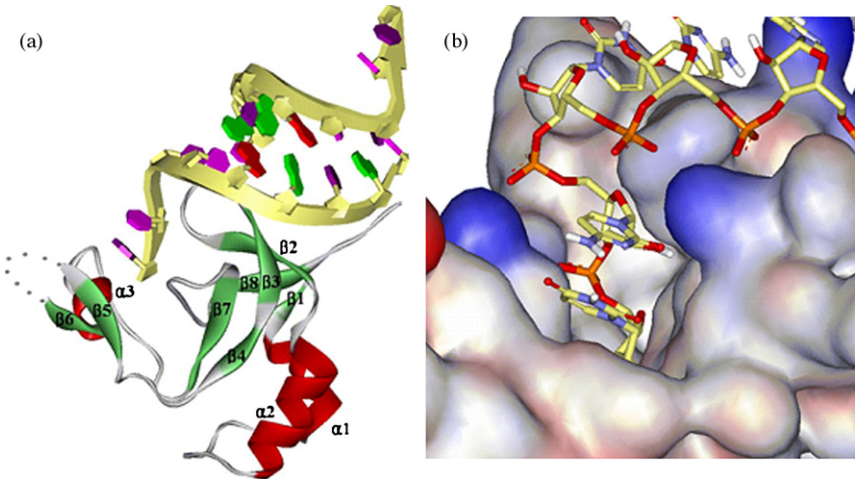

Fig. 1. The structure of PAZ/siRNA-like duplex complex. (a) Ribbon presentation of the backbone atoms of the PAZ domain and the siRNA-like duplex. (b) Detail of the 2 nt 3′-overhang of siRNA molecules positioned in the binding pocket of the PAZ domain. The siRNA-like duplex is shown in a stick representation. The PAZ domain is depicted in an electrostatic surface representation, with blue and red colors corresponding to the positively and negatively charged groups, respectively.

helix α3, strand β5 along one face, the residues between strand β7 and β8, and loop β2–β3 along the opposite face. The 2 nt 3′-overhang of siRNA molecules is positioned in this binding pocket (Fig. 1b). The interactions between the PAZ domain and two strands of siRNA are highly asymmetric. The strand with its 3′-overhang contacting the PAZ domain is involved in the majority of contacts between the PAZ domain and the siRNA, whereas the complementary strand contacts only with its 5′ end residue [13]. These structural characteristics of the PAZ domain indicate that it may contribute to the specific and productive incorporation of siRNAs into the RNAi pathway [12–14].

In this study, we investigated the interaction between the PAZ domain and siRNAs using a computer simulation technique. Through the dissociation molecular dynamics (DMD) simulations, we obtained information regarding various physical properties during the possible dissociation processes of the PAZ domain and the siRNAs. Especially, we compared the responses of the PAZ domain to various 3′-overhang structures of the siRNAs.

2. Methodology

2.1. Modeling of PAZ domain

The starting structure for simulation was the 2.6 Å crystal structure of the PAZ domain from human Argonaute eIF2c1 bound with a 9 nt siRNA-like duplex (PDB entry 1SI3) (Fig. 1) [13]. We denote the strand with 3′-overhang contacting the PAZ domain and its complementary strand as strand 1 and strand 2, respectively. Only the structure spanning from Ala225 to Arg349 of the PAZ domain was used. The N and C termini were capped with the neutral acetyl and the *N*-methyl group, respectively. The protein was represented by the CHARMM 19 polar hydrogen model [15]. All charges were set to those corresponding to pH 7; Arg and Lys residues were positively charged, Asp and Glu residues negatively charged and the His residue was neutralized. The loop (six residues from Leu296 to Thr301 between strand β5 and β6), which does not appear on the X-ray crystal structure, was modeled by MODELLER version 6.2 [16]. To optimize the modeled loop, the initial structure of the PAZ domain containing the modeled loop was subjected to a steepest descent energy minimization of 1000 iterations, in which the coordinates of all atoms except for those in the loop were fixed.

2.2. Modeling of siRNA-like duplex

RNA polar hydrogen topology was used to model the siRNA-like duplex. The bond parameters were obtained from CHARMM 10_22 parameters [17]. The van der Waals interactions of the original CHARMM nucleic acid polar hydrogen model were calculated using the Slater and Kirkwood equation. In order to apply CHARMM 19 potential function, we used the Lorentz–Berthelot simple mixing rules [18], rather than the Slater and Kirkwood equation [19]. The van der Waals interaction parameters of the RNA atoms were obtained from similar atoms in the CHARMM 19 parameter file, with the exception of the phosphorus atom, whose parameters were from the CHARMM 27 parameter file [20]. The CHARMM nucleic acid polar hydrogen model also includes an explicit hydrogen bond term. The CHARMM 19 potential function does not include an explicit hydrogen bond term, so it was determined through a revision of the partial atomic charges, so as to obtain hydrogen bonding interactions consistent with *ab initio* calculations [15]. The partial atomic charges for siRNA-like duplex molecules were revised to exclude the hydrogen bond term. These parameters were obtained from the partial atomic charges of the CHARMM 27 topology file. The partial charges of united atoms were parameterized by the summation of the partial charges of the atoms included in the groups. The partial charges of the positively charged atoms of the ionic groups were increased to obtain higher polarities of the ionic groups and to make them neutral (resulting modified parameters are listed in the supplementary material).

The original siRNA-like duplex had three non-complementary base pairs in its A-form duplex and hydroxyl group at 5′ end

of strand 2. We modified these base pairs into complementary base pairs and substituted the hydroxyl group for phosphate group to make a more realistic siRNA-like duplex structure. In order to maintain the native A-helical conformation of RNA duplex and remove uninteresting degrees of freedom in the double helix during DMD simulations, the harmonic potential was applied to nonbonded interaction pairs consisting of two $C4^*$ atoms in RNA duplex (force constant value was 5 kcal/mol Å^2).

Additional optimization of the nonbond interaction parameter of RNA molecules was performed because the parameters of the molecules were obtained from different CHARMM parameter files. We recalibrated the partial atomic charges of the RNA molecules by various scaling factors and then compared the structural stability of the original structures. The structural stabilities of the complex were measured by the average pair contact deviation P_{rmsd} at the binding interface between the PAZ domain and siRNA-like duplex during 50 ps MD simulation (The energy-minimized structures were heated to 298.0 K for 12 ps and equilibrated for 38 ps.). P_{rmsd} is defined as follows:

$$P_{\mathrm{rmsd}} = \left(\frac{1}{{}_N C_2} \sum_{i=1}^{N-1} \sum_{j=i+1}^{N} (r_{ij} - r_{0,ij})^2 \right)^{1/2} \quad (1)$$

where ${}_N C_2$ is a combination selecting two different atoms without considering their order, r_{ij} is the distance between i and j atom of simulated structures and $r_{0,ij}$ is the distance between i and j atom at t_0. N is the sum of the number of CA atoms of the PAZ domain within the binding interface and the number of $C4^*$ atoms of RNA. Only CA–$C4^*$ atom pairs of PAZ domain and siRNA-like duplex within 9 Å were considered to reduce the calculation cost. The $C4^*$ atoms and the CA atoms were selected because they are roughly geometric centers of each residues. Based on the 50 ps MD simulation results (data not shown), we chose the scaling factor, 0.985 at which the structure had the lowest P_{rmsd} value and the RNA partial atomic charges scaled by this scale factor were used in all simulations reported herein.

The 3′-overhang was modified with several other structures, such as blunt end, U, UU, CC, AA and GG. These modified structures are denoted as blunt end, P-siR-U, P-siR-UU, P-siR-CC, P-siR-AA and P-siR-GG, respectively.

2.3. Energy function

The CHARMM 19 potential function with the implicit solvation model EEF1 [21] was used in this study. The implicit solvation model used in our study assumes that the solvation free energy of a polyatomic solute is the sum over group contributions. The solvation free energy of each group is the solvation free energy of that group in small model compounds minus the amount of solvation it loses due to the exclusion of the solvent by other protein atoms around it.

$$\Delta G^{\mathrm{slv}} = \sum_i \Delta G_i^{\mathrm{slv}} = \sum_i \Delta G_i^{\mathrm{ref}} - \sum_i \sum_{j \neq i} f_i(r_{ij}) V_j \quad (2)$$

where $\Delta G_i^{\mathrm{slv}}$ is the solvation free energy of group i and $\Delta G_i^{\mathrm{ref}}$ are the reference solvation free energy of group i fully exposed to the solvent, $f_i(r_{ij})$ is a solvation free energy density function and V_j the volume of group j. The solvation parameters of the siRNA-like duplex atoms were obtained from similar atoms in EEF1.

2.4. Dissociation MD simulation and analysis

In DMD simulations, the bound siRNA-like duplex was pulled out of the PAZ domain using an artificial biasing perturbation. If the biasing perturbation for the dissociation process is applied to an atom of one domain and the other atom of its bound domain, the equilibrium dissociation pathway might be seriously influenced by the positions of the selected atoms. To avoid this problem, we applied the biasing perturbation between the center of mass (CM) of the PAZ domain and that of the siRNA-like duplex. The perturbation has the form:

$$W_{\mathrm{bias}} = k_{\mathrm{CMC}}(R - R_{\mathrm{C}})^2 \quad (3)$$

where W_{bias} is the biasing potential energy in kcal/mol, k_{CMC} the spring constant, R the distance between the position vectors of CMs of the A domain and the B domain ($R = |\mathbf{R}_{\mathrm{A,CM}} - \mathbf{R}_{\mathrm{B,CM}}|$), and R_{C} the constraint length between the two CMs. In our DMD simulation model, the biasing force was assigned to the CA atoms of PAZ domain and the $C4^*$ atoms of siRNA-like duplex. The R_{C} was fixed at 0.03 Å/ps and k_{CMC} was set at 0.5 kcal/(mol Å^2).

The inter-domain distance was defined as the distance between the position vectors of the CMs of the PAZ domain and the siRNA-like duplex. The inter-domain effective energy W_{inter} was calculated using the equation:

$$W_{\mathrm{inter}} = E_{\mathrm{vdW,inter}} + E_{\mathrm{El,inter}} + \Delta G^{\mathrm{deslv,inter}} \quad (4)$$

where $E_{\mathrm{vdW,inter}}$ is van der Waals energy, $E_{\mathrm{El,inter}}$ electrostatic energy and $\Delta G^{\mathrm{deslv,inter}}$ the inter-domain desolvation free energy change. The desolvation energy change is due to the solvent exclusion effect by binding of the PAZ domain and the siRNA-like duplex. The DMD simulations were performed for 1.3 ns.

2.5. Molecular dynamics simulation protocol

All simulations with an integration step of 2 fs and data analyses were performed using an in-house developed MD simulation program, named SELF-ASSEMBLER [22]. The entire structure of PAZ/siRNA-like duplex was subjected to a steepest descent energy minimization of 500 iterations. The bond lengths involving hydrogen atoms were fixed with a SHAKE algorithm [23]. During both energy minimization and molecular dynamics, the nonbonded forces were truncated at 11 Å using an electrostatic shifting function and a van der Waals switching function [24]. Nonbonded interactions were processed using a 13 Å list, updated every 25 steps. Coordinates were saved every 500 steps. The temperature of the system was maintained at 298.0 K using a Berendsen thermostat [25] with $\tau_{\mathrm{T}} = 0.1$ ps.

3. Results

3.1. Structural stability during MD simulations

All models were initially equilibrated by MD simulations without a biasing perturbation for 1 ns in which the energy-minimized structures were gradually heated for 60 ps and equilibrated for 940 ps. Fig. 2a shows the average pair contact deviation, P_{rmsd}, of the P-siR-GG model at the binding interface versus time. As shown in the plots, P_{rmsd} was stable with modest fluctuations during the equilibration. Fig. 2b shows the number of hydrogen bonds between the PAZ domain and strand 1 of the siRNA-like duplex versus time. The number of hydrogen bonds rapidly increased at the beginning of the simulation and then gradually decreased into that in the experimental structure. These results demonstrate that our simulation methods with the modified force field can be used for the modeling of the PAZ domain bound with the siRNA-like duplex.

Fig. 3a shows the total energy of the PAZ domain during the equilibrium MD simulations. The average total energy values for the PAZ domains in the absence and presence of siRNA-like duple are −2900 and −2805 kcal/mol, respectively. DMD simulations with high pulling velocity may lead to the increase of the total energy due to the structural instability of the PAZ domain, which may result in serious simulation artifacts.

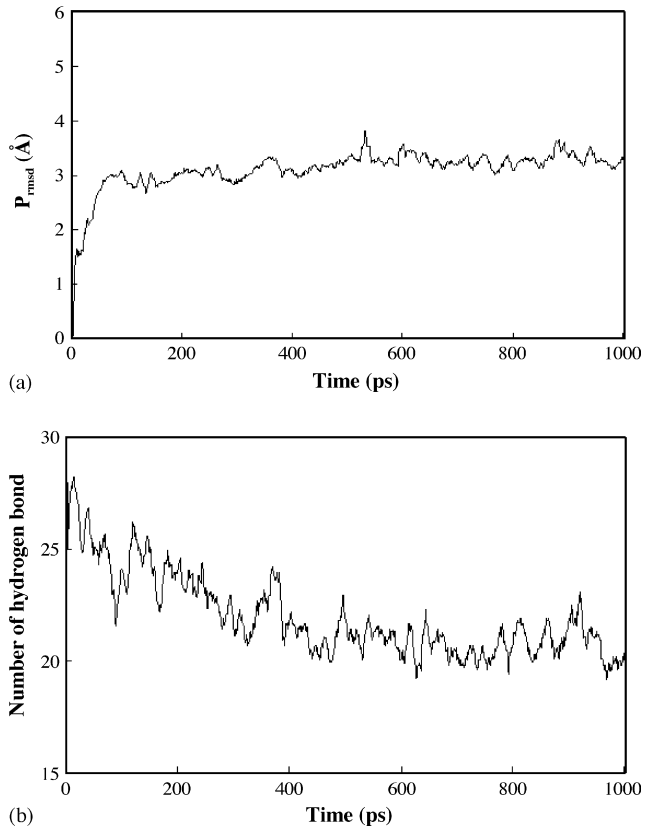

Fig. 2. Structural stability of the model during equilibrium simulations. (a) The average pair contact deviation, P_{rmsd}, at the binding interface between the PAZ domain and the P-siR-GG. (b) The number of hydrogen bonds of strand 1 for the siRNA-like molecule.

Fig. 3b shows that the total energy of the PAZ domain was maintained during the DMD simulations in a range within the average total energy values obtained from the equilibrium MD simulations of Fig. 3a, suggesting our pulling velocity is in an acceptable value.

3.2. Effect of 5′-phosphate substitution on PAZ domain structure

The ribonuclease III enzyme, Dicer, generates ∼20 nt dsRNA duplexes with 5′ phosphate and 3′ hydroxyl groups

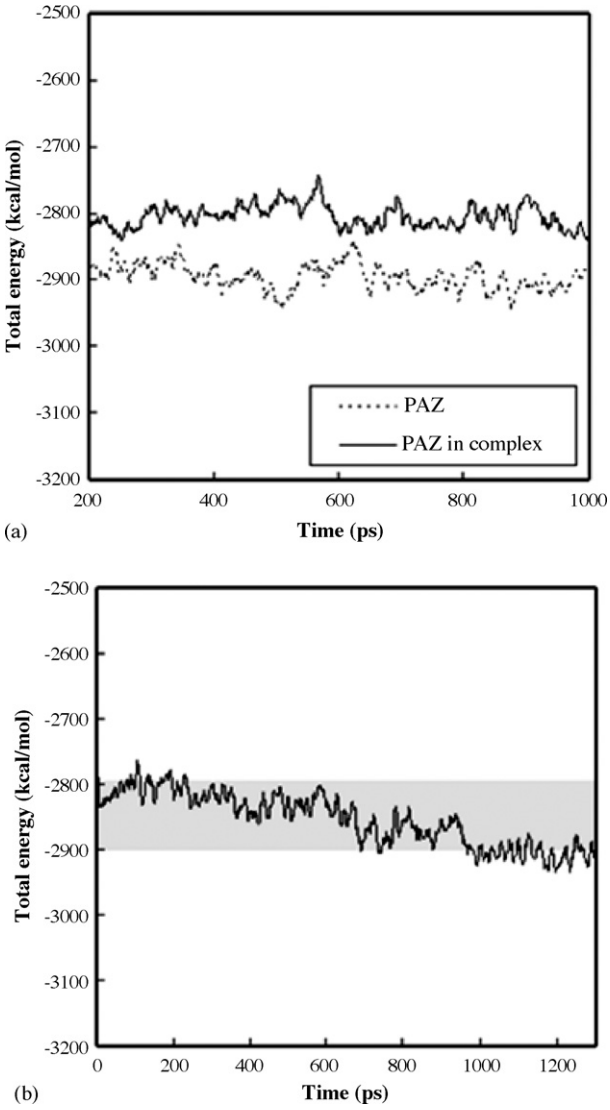

Fig. 3. Structural stability of the model during DMD simulations. (a) The total energy of the PAZ domain during the equilibrium period. The total energy is the total effective energy value which is given the sum of the bonded energy, the van der Waals energy, the electrostatic energy, and the solvation free energy. 'PAZ' (dashed line) denotes the total energy obtained from the equilibrium MD simulation for the PAZ domain in the absence of siRNA-like duplex. 'PAZ in complex' (solid line) is the contribution of the PAZ domain to the total energy of PAZ/siRNA-like duplex, P-siR-GG during the equilibrium MD simulation. (b) The total energy changes of the PAZ domain during the DMD simulation for P-siR-GG. The section between two average total energy values of the PAZ domain calculated from a is highlighted in light gray.

from a long dsRNA. In the case of synthetic siRNAs containing 5′ hydroxyl group, these hydroxyl groups are rapidly phosphorylated [26]. Nykänen et al. [27] reported that in the *Drosophila*, an endogenous kinase rapidly converts the 5′ hydroxyl group to a phosphate. 5′ hydroxyl-containing, synthetic siRNAs that trigger RNAi in cultured mammalian cells, mice, and perhaps even in plants may likewise be phosphorylated by a cellular kinase prior to entering the RNAi pathway. Therefore, the 5′ hydroxyl group of the RNA strand contacted with the PAZ domain was substituted for a phosphate group in our simulations.

Fig. 4 shows the original structure and a snapshot of 5′-end phosphate-substituted model structure after the equilibrium MD simulation. The PAZ domain of the original structure does not contact the 5′-hydroxyl group of strand 2 (Fig. 4a). In the 5′-end phosphate-substituted structures, the negatively charged oxygen atoms of 5′-end phosphate groups closely interacted with two positively charged residues, Lys274 and Lys276 (Fig. 4b). These interactions are due to the higher negativity of the phosphate group than that of the hydroxyl group. Masunov and Lazaridis reported that, in their EEF1 model, the polarity of the pseudoionic side chain is too strong so the interactions within residues are too attractive [28]. The observed conformational change could be an artifact resulting from the EEF1 solvation model employed in our potential functions. Considering the relatively short distances between 5′-end and the Lys residues, however, we propose that the 5′-phosphate of the complementary strand might contribute to the molecular recognition process of the binding of siRNA to the PAZ domain.

3.3. 2 nt 3′-overhang sequence effect

Fig. 5a is a profile of the magnitude of the perturbation, called bias energy hereafter, as a function of simulation time for four models with different 2 nt 3′-overhang sequences. The bias energy plays a role in shortening the times during which the binding energy is trapped in a local minimum, thereby accelerating the dissociation processes of this complex. An increase of the bias energy indicates that the dissociation of the PAZ domain and siRNA-like duplex takes place slowly, if detectable, and the external perturbation is accumulated. A decrease in the bias energy means that breaking the interactions between these two molecules occurs, and the external perturbation is released. The bias energy profile in this plot shows multiple strong peaks, suggesting that various inter-domain interactions are involved in the binding of the PAZ domain and siRNA-like duplex. The simulation results also show that P-siR-UU had the largest bias energy before the first large drop of the bias energy. This feature implies that the complex with 3′ UU-overhang has relatively high structural stabilities compared to other complexes. Fig. 5b is inter-domain distances as a function of simulation time for these four models. The rapid increases of the inter-domain distance corresponded well with the rapid drops in the bias energy.

Fig. 6 shows the profiles of the distances between the position vectors of the CMs of PAZ domain binding pocket and 2 nt 3′-overhangs as a function of time. The position vector of the CM of the pocket was calculated using CA atoms located within 7 Å from the $C4^{*}$ atoms of the 2 nt overhangs in equilibrated crystal structure. The results show that the UU-overhang lodged in the binding pocket of the PAZ domain the longest among the four different overhangs during the DMD simulations. The distance profile of the pocket/3′-overhang was clearly different from the inter-domain distance profiles of PAZ/siRNA-like duplex plotted in Fig. 5b. The inter-domain distance of P-siR-UU increased rapidly at ∼630 ps, whereas no rapid increase was observed in the distance of pocket/3′-overhang, except for small fluctuations. The results of Figs. 5b and 6 suggest that the PAZ domain and siRNA-like duplexes do not dissociate in a synchronous manner. The first seven base pairs of the strands are separated from their contacting PAZ domain prior to the separation of the 3′-overhangs. This implies that 3′-overhang makes the strongest contact with the PAZ domain. A similar result was observed in the total inter-domain effective energy and the 3′-overhang inter-domain effective energy as plotted in Fig. 7. Once the structural stability began to be impaired at about 600 ps, the total inter-domain effective

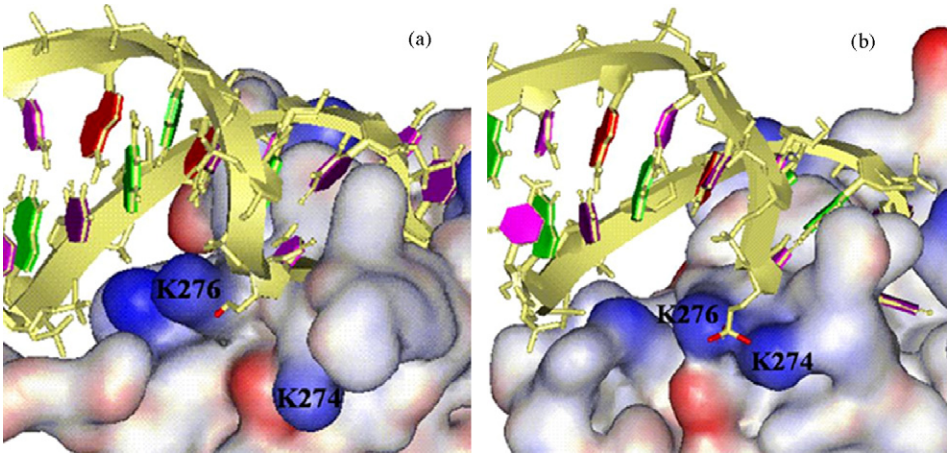

Fig. 4. Interaction between the positively charged residues (K274 and K276) and the 5′-end phosphate group. (a) Original structure with the 5′-hydroxyl group. (b) A snapshot after equilibration for the 5′-end phosphate-substituted P-siR-UU model structure.

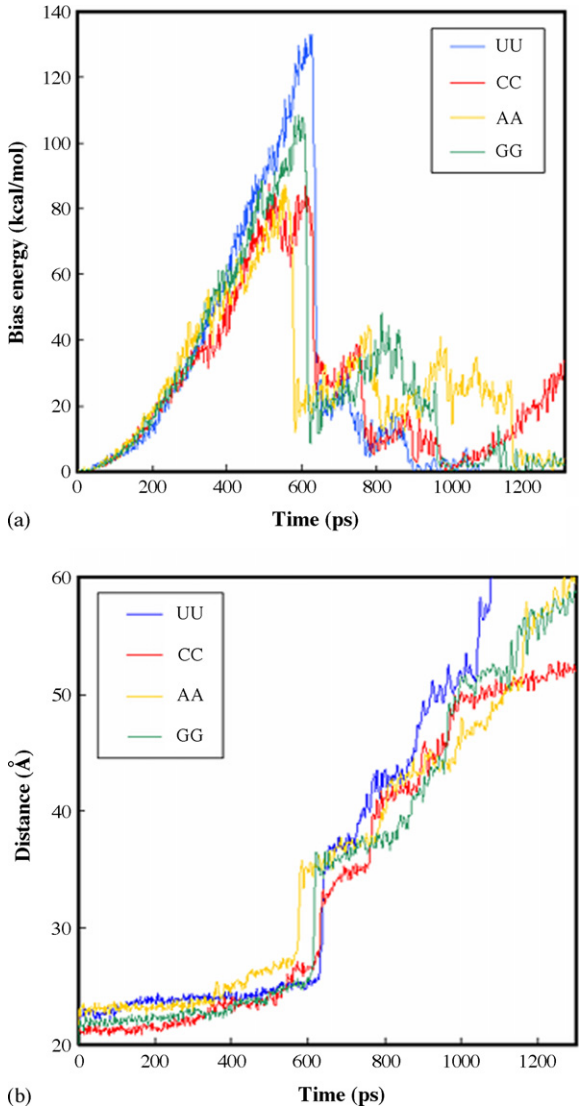

Fig. 5. Bias energy and inter-domain distance profiles as a function of time for PAZ/siRNA-like duplex models with four different 3′-overhangs under the distance constraint between the two molecules. (a) Changes in the bias energies. (b) Changes in the distances between the position vectors of the CMs of the PAZ domain and the siRNA-like duplex.

energy was mainly contributed by the 3′ overhang inter-domain effective energy.

There was a difference between the inter-domain effective energies of the P-siR-UU and the others. In the P-siR-UU, the residual effective energy between the PAZ domain and 3′-overhang totally disappeared after ∼1085 ps. It means that the PAZ domain and the siRNA-like duplex were completely separated from each other, which did not happen for others until the end of our simulations. Based on the changes of the inter-domain effective energies, we divided the dissociation process into three phases. Phase I is a period in which the total and overhang effective energies remain almost constant or are slightly reduced. In phase II, the total inter-domain effective energy begins to decrease rapidly and then reaches the overhang effective energy. In phase III, the residual effective energy from the interactions between overhang and

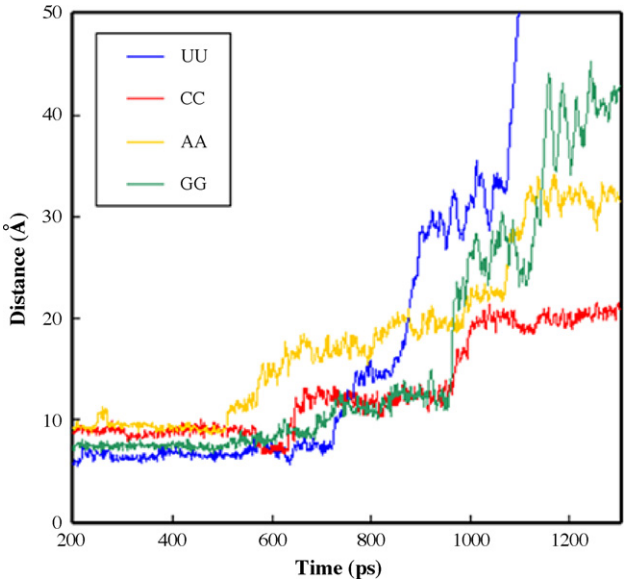

Fig. 6. Profiles of the distances between the position vectors of the CMs of the pocket and the 3′-overhangs as a function of time. The pocket is the binding site of the PAZ domain consisting of the residues that interact with the 3′-overhang of the siRNA-like duplex in equilibrated crystal structure.

the PAZ domain gradually decreases and eventually disappears. The plots of the inter-domain effective energies show that the P-siR-UU has the shortest phase II and III. The overhangs do not interact only within the binding pocket, but mainly with residues outside once the overhangs begin to dislodge from the binding pocket. The results of Figs. 6 and 7 indicate that the P-siR-UU had the shortest retention time outside of the binding pocket in the PAZ domain during phase II and III.

The interaction regions between the PAZ domain and the siRNA-like duplex can be divided primarily into three parts; RNA duplex segment of the strand 1 (region 1), 5′-terminus of the strand 2 (region 2) and the 2 nt 3′-overhang segment (region 3) with the PAZ domain (Fig. 8a). We carried out the analysis of the number of hydrogen bonds formed or broken at each region during the DMD simulations (Fig. 8b). The sharp decrease of the bias energies were closely correlated to the number of hydrogen bonds at the three regions. In the P-siR-UU, for example, the largest drop at ∼630 ps, small drops at ∼730 ps and at ∼860 ps were due to the breakage of hydrogen bonds after the accumulation of perturbation energy at region 1, 2 and 3, respectively. These sequential breakages of hydrogen bonds at the three regions were similarly observed in the P-siR-CC, the P-siR-AA and the P-siR-GG as well, though the details of the hydrogen bond breakage were somewhat different from each other. During phase II and III, the number of hydrogen bonds by the 2 nt 3′-overhang of the P-siR-UU decreased more rapidly than those of the different overhangs. Two uracils have six hydrogen bonding donors or acceptors, whereas two cytosines, two adenines, and two guanines have eight, ten, and twelve, respectively. The short retention time of the UU-overhang may be due to the smallest number for the hydrogen bonding of the uracil, resulting in weak interactions between the UU-overhang and the protein.

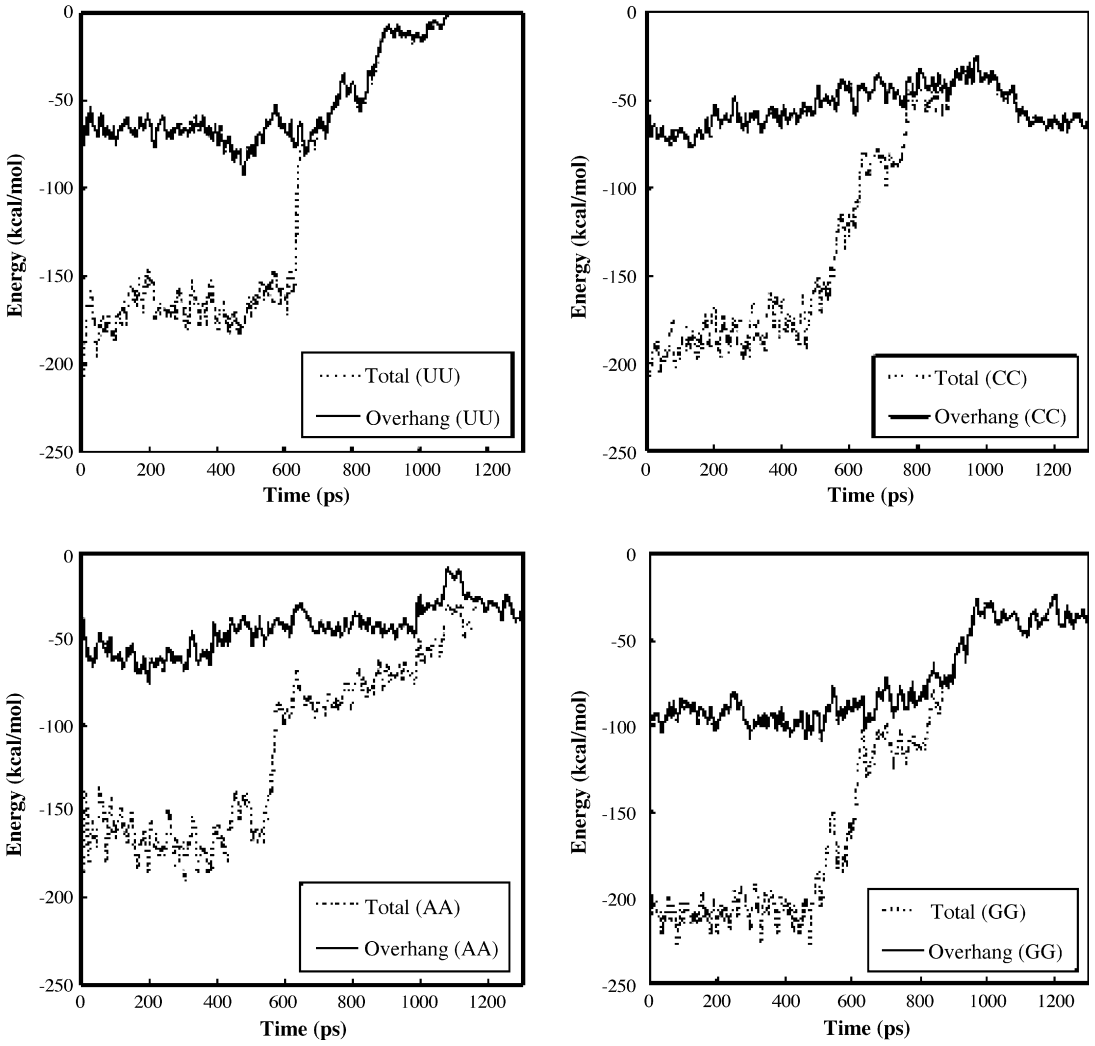

Fig. 7. Changes in the inter-domain effective energy as a function of time for P-siR-UU, P-siR-CC, P-siR-AA and P-siR-GG. 'Overhang' denotes the inter-domain effective energy between the PAZ domain and the 3′-overhang. 'Total' denotes the inter-domain effective energy interacting between the PAZ domain and the whole siRNA-like duplex.

3.4. 3′-overhang length effect

The binding pocket in the PAZ domain provides a unique mode for the recognition of the characteristic two nucleotide 3′ overhang [13,29]. siRNA with a deficient overhang, such as 1 nt or blunt end, would be hard to form a specific complex with the PAZ domain due to the disability of the overhang in recognizing the binding pocket of the PAZ domain at an early stage of the binding process. Binding affinity of the complex with 1 nt 3′-overhang measured by Ma et al. was a value reduced by 85-fold compared with 2 nt 3′-overhang. As two 3′-nucleotides were removed, the binding affinity reduced by >5000-fold [13].

We examined how the complexes of PAZ/siRNA-like duplexes with the deficient overhangs responded to the applied external perturbation during DMD simulations. The results showed that the maximum bias energy increases as the length of 3′-overhang decreases (Fig. 9). This indicates that the 2 nt overhang contributes to the facilitated separation of the siRNA-like duplex from the PAZ domain.

4. Discussion and conclusion

The simulation results have revealed that the siRNA with UU-overhang can form the PAZ/siRNA complex with a relatively high stability but readily separate from the PAZ domain once the structural stability of the complex is impaired by external perturbations (Table 1).

Ma et al. carried out a surface plasmon resonance experiment for RNA duplexes with UU and AG 3′-overhangs [13]. Their results showed that the apparent dissociation constant of RNA duplexes with UU-overhang was larger than that with AG overhang. The PAZ domains dissociated more rapidly from the RNA duplexes with UU-overhang than those with AG-overhang though the PAZ domains bound more to the RNA duplexes with UU-overhang at a high concentration during the association period. This paradoxical result can be explained nicely by our simulation results.

According to our DMD simulation results for the complexes of PAZ/siRNA-like duplexes with the different lengths of overhangs, 2 nt overhang is also likely to contribute more to

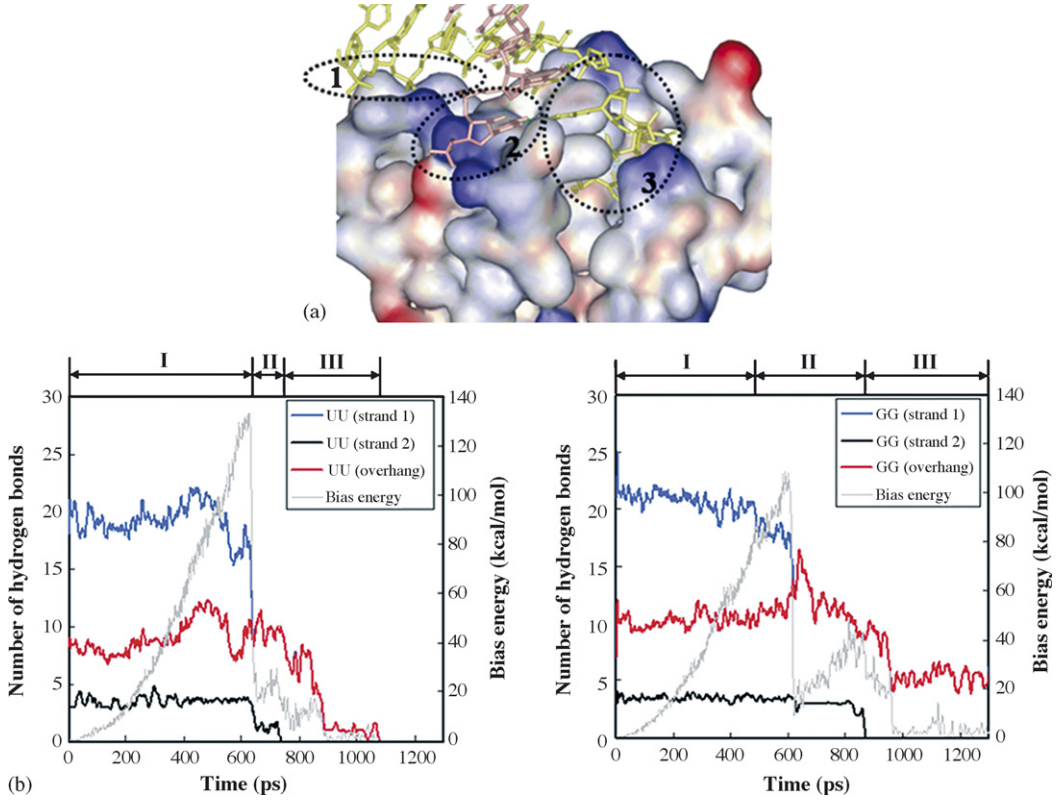

Fig. 8. Analysis of the number of hydrogen bonds. (a) A magnified view at the inter-domain binding surface. The PAZ domain and the siRNA-like duplex are shown in electrostatic surface representation and stick representation, respectively. Strand 1 and strand 2 in the siRNA-like duplex are shown by different colors. Three interaction regions are depicted by dashed circles. (b) The changes of the number of hydrogen bonds formed between the PAZ domain and the siRNA-like duplex during the DMD simulation are plotted. The hydrogen bonds by strand 1, strand 2 and 3′-overhang of strand 1 are shown as blue, black and red line, respectively. The bias energy (gray line) is displayed for a reference. I, II and III denote the three different phases during the dissociation pathway. Plots for the P-siR-UU and the P-siR-GG are on the left and the right, respectively.

facilitating the separation of the siRNA duplex from the bound PAZ domain compared to 1 nt overhang and blunt end. Energetically most favorable UU-overhang has the lowest maximum bias energy during the DMD simulations. This indicates that the strength of the interaction by overhang in the binding pocket can influence the structural stability of the PAZ/siRNA complex in a condition that external perturbations are applied.

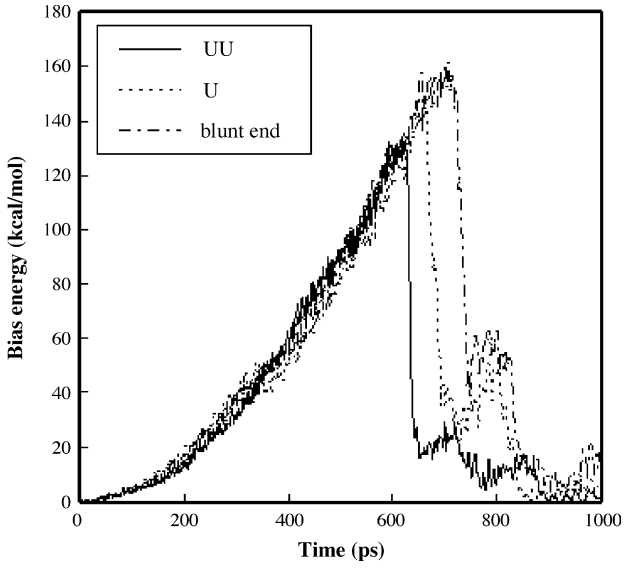

Fig. 9. Changes in the bias energies for PAZ/siRNA-like duplex models with three different lengths of 3′-overhangs as a function of time during DMD simulations.

The efficiency of RNA interference are governed by several factors, such as, for the siRNA, to enter Dicer or Argonaute protein, to be transferred from the Dicer, to recognize the target sequences in the activated RISC, and to release the cleaved product. For Argonaute function in the RISC, Tomari and Zamore proposed a "two-state" model [30]. The 2 nt 3′-overhang of the guide strand of siRNA is buried deep in the binding pocket of the PAZ domain in Argonaute in a way that prohibits its base pairing with the target RNA [13]. In the two-state model, the force propagated through the base pairing

Table 1
Comparison of four PAZ/siRNA-like duplex models with different 3′-overhang sequences

3′-overhang	Bias energy (kcal/mol)	t_1 (ps)	t_2 (ps)
UU	123	633	1116
CC	69	440	>1300
AA	87	505	>1300
GG	101	607	>1300

Bias energy is the magnitude of accumulated external perturbation at a simulation time, t_1 when the first large structural instability between two molecules is observed. t_2 is a simulation time when two molecules are completely separated. The values are obtained by averaging over three independent runs.

between the 5′ region of the guide strand and target RNA would lead the 3′ region of the guide strand to dislodge from the PAZ domain and to make base-pairing with the target RNA in the PIWI domain. The 3′ region of the guide strand would re-anchor to the PAZ domain with the release of the cleaved target RNA. If the two-state model is right, the rates of dislodging and lodging between the PAZ domain and the guide strand for multiple cleavage rounds might be an important factor determining RNAi efficiency.

To get an insight into the association process between the PAZ domain and siRNA, we imagined backward pathways of the dissociations. At the initial stage of binding of the two molecules, an siRNA might bind to the periphery of the binding pocket and then probe into the pocket of the PAZ domain. This process would be an essential step to form geometrically matching and structurally stable complexes. We speculate that the UU-overhang's short retention time at the outside of the binding pocket might help the siRNA to bind promptly to its binding pocket and rapidly form the structurally stable complex because it might spend less time searching for the binding pocket.

Although several simplifications and artificial constraints in our simulation methods might produce simulational artifacts or unphysical pathways during the dissociation between the PAZ domain and the siRNA-like duplex, the present work provides an interesting dissociation mechanism derived from a computer simulation. In summary, our simulation results show that the structures of 3′-overhangs may influence the dissociation process between the PAZ domain and siRNAs. Among the siRNAs with four different consecutive 2 nt overhang structures, the siRNA with UU-overhang form a relatively high stable complex with the PAZ domain but separate from the PAZ domain most rapidly once the stable binding structure of these two molecules is broken by external perturbations. We suggest that these characteristics of the UU-overhang siRNA observed from our simulations might contribute to the high efficiency of RNAi.

Acknowledgments

This study was supported by grants to H. Lee (A05-0185) from the Ministry of Health & Welfare and to H. Choe (2003-307 and 2004-307) from the Asan Institute for Life Sciences, Seoul, Korea.

Appendix A. Supplementary data

Supplementary data associated with this article can be found, in the online version, at doi:10.1016/j.jmgm.2006.07.002.

Appendix A. Supplementary data

References

[1] A. Fire, S. Xu, M.K. Montgomery, S.A. Kostas, S.E. Driver, C.C. Mello, Potent and specific genetic interference by double-stranded RNA in *Caenorhabditis elegans*, Nature 391 (1998) 806–811.

[2] R.F. Ketting, S.E. Fischer, E. Bernstein, T. Sijen, G.J. Hannon, R.H. Plasterk, Dicer functions in RNA interference and in synthesis of small RNA involved in developmental timing in *C. elegans*, Genes Dev. 15 (2001) 2654–2659.

[3] S.W. Knight, B.L. Bass, A role for the RNase III enzyme DCR-1 in RNA interference and germ line development in *Caenorhabditis elegans*, Science 293 (2001) 2269–2271.

[4] S.M. Elbashir, J. Harborth, W. Lendeckel, A. Yalcin, K. Weber, T. Tuschl, Duplexes of 21-nucleotide RNAs mediate RNA interference in cultured mammalian cells, Nature 411 (2001) 494–498.

[5] S.M. Elbashir, W. Lendeckel, T. Tuschl, RNA interference is mediated by 21- and 22-nucleotide RNAs, Genes Dev. 15 (2001) 188–200.

[6] S.M. Elbashir, J. Martinez, A. Patkaniowska, W. Lendeckel, T. Tuschl, Functional anatomy of siRNAs for mediating efficient RNAi in *Drosophila melanogaster* embryo lysate, Embo J. 20 (2001) 6877–6888.

[7] S.M. Hammond, E. Bernstein, D. Beach, G.J. Hannon, An RNA-directed nuclease mediates post-transcriptional gene silencing in *Drosophila* cells, Nature 404 (2000) 293–296.

[8] J. Martinez, A. Patkaniowska, H. Urlaub, R. Luhrmann, T. Tuschl, Single-stranded antisense siRNAs guide target RNA cleavage in RNAi, Cell 110 (2002) 563–574.

[9] M.A. Carmell, Z. Xuan, M.Q. Zhang, G.J. Hannon, The Argonaute family: tentacles that reach into RNAi, developmental control, stem cell maintenance, and tumorigenesis, Genes Dev. 16 (2002) 2733–2742.

[10] J.J. Song, S.K. Smith, G.J. Hannon, L. Joshua-Tor, Crystal structure of Argonaute and its implications for RISC slicer activity, Science 305 (2004) 1434–1437.

[11] E. Bernstein, A.A. Caudy, S.M. Hammond, G.J. Hannon, Role for a bidentate ribonuclease in the initiation step of RNA interference, Nature 409 (2001) 363–366.

[12] J.J. Song, J. Liu, N.H. Tolia, J. Schneiderman, S.K. Smith, R.A. Martienssen, G.J. Hannon, L. Joshua-Tor, The crystal structure of the Argonaute2 PAZ domain reveals an RNA binding motif in RNAi effector complexes, Nat. Struct. Biol. 10 (2003) 1026–1032.

[13] J.B. Ma, K. Ye, D.J. Patel, Structural basis for overhang-specific small interfering RNA recognition by the PAZ domain, Nature 429 (2004) 318–322.

[14] K.S. Yan, S. Yan, A. Farooq, A. Han, L. Zeng, M.M. Zhou, Structure and conserved RNA binding of the PAZ domain, Nature 426 (2003) 468–474.

[15] E. Neria, S. Fischer, M. Karplus, Simulation of activation free energies in molecular systems, J. Chem. Phys. 105 (1996) 1902–1921.

[16] M.A. Marti-Renom, A.C. Stuart, A. Fiser, R. Sanchez, F. Melo, A. Sali, Comparative protein structure modeling of genes and genomes, Annu. Rev. Biophys. Biomol. Struct. 29 (2000) 291–325.

[17] L. Nilsson, M. Karplus, Empirical energy functions for energy minimizations and dynamics of nucleic acids, J. Comp. Chem. 7 (1986) 591–616.

[18] M.P. Allen, D.J. Tildesley, Computer simulation of liquids, Clarendon, Oxford, 1987.

[19] J.C. Slater, J.G. Kirkwood, The van der Waals forces in gases, Phys. Rev. 37 (1931) 682–697.

[20] A.D. MacKerell Jr., N. Banavali, All-atom empirical force field for nucleic acids. 2: application to molecular dynamics simulations of DNA and RNA in solution, J. Comp. Chem. 21 (2000) 105–120.

[21] T. Lazaridis, M. Karplus, Effective energy function for proteins in solution, Proteins 35 (1999) 133–152.

[22] H.S. Lee, R.C. Robinson, C.H. Joo, H. Lee, Y.K. Kim, H. Choe, Targeted molecular dynamics simulation studies of calcium binding and conformational change in the C-terminal half of gelsolin, Biochem. Biophys. Res. Commun. 342 (2006) 702–709.

[23] J.P. Ryckaert, G. Cicotti, H.J.C. Berensden, Numerical integration of the Cartesian equations of motion of a system with constraints: molecular dynamics of *n*-alkanes, J. Comp. Phys. 23 (1977) 237–341.

[24] C.L. Brooks, B.M. Pettitt, M. Karplus, Structural and energetic effects of truncating long ranged interactions in ionic and polar fluids, J. Chem. Phys. 83 (1985) 5897–5908.

[25] H.J.C. Berendsen, J.P.M. Postma, W.F. van Gunsteren, A. DiNola, J.R. Haak, Molecular dynamics with coupling to an external bath, J. Chem. Phys. 81 (1984) 3684–3690.

[26] D.S. Schwarz, G. Hutvagner, B. Haley, P.D. Zamore, Evidence that siRNAs function as guides, not primers, in the *Drosophila* and human RNAi pathways, Mol. Cell 10 (2002) 537–548.
[27] A. Nykanen, B. Haley, P.D. Zamore, ATP requirements and small interfering RNA structure in the RNA interference pathway, Cell 107 (2001) 309–321.
[28] A. Masunov, T. Lazaridis, Potential of mean force between ionizable amino acid side chains in water, J. Am. Chem. Soc. 125 (2003) 1722–1730.
[29] A. Lingel, B. Simon, E. Izaurralde, M. Sattler, Nucleic acid 3′-end recognition by the Argonaute 2 PAZ domain, Nat. Struct. Mol. Biol. 11 (2004) 576–577.
[30] Y. Tomari, P.D. Zamore, Perspective: machines for RNAi, Genes Dev. 19 (2005) 517–529.